

Transport gap in suspended bilayer graphene at zero magnetic fieldA. Veligura,^{1,*} H. J. van Elferen,² N. Tombros,¹ J. C. Maan,² U. Zeitler,² and B. J. van Wees¹¹*Physics of Nanodevices, Zernike Institute for Advanced Materials, University of Groningen, Nijenborgh 4, 9747 AG Groningen, The Netherlands*²*High Field Magnet Laboratory and Institute for Molecules and Materials, Radboud University Nijmegen, Toernooiveld 7, 6525 ED Nijmegen, The Netherlands*

(Received 8 February 2012; revised manuscript received 23 March 2012; published 5 April 2012)

We report a change of three orders of magnitude in the resistance of a suspended bilayer graphene flake which varies from a few k Ω in the high-carrier-density regime to several M Ω around the charge neutrality point (CNP). The corresponding transport gap is 8 meV at 0.3 K. The sequence of quantum Hall plateaus appearing at filling factor $\nu = 2$ followed by $\nu = 1$ suggests that the observed gap is caused by the symmetry breaking of the lowest Landau level. Investigation of the gap in a tilted magnetic fields indicates that the resistance at the CNP shows a weak linear decrease for increasing total magnetic field. Those observations are in agreement with a spontaneous valley splitting at zero magnetic field followed by splitting of the spins originating from different valleys with increasing magnetic field. Both the transport gap and B field response point toward the spin-polarized layer-antiferromagnetic state as the ground state in the bilayer graphene sample. The observed nontrivial dependence of the gap value on the normal component of B suggests possible exchange mechanisms in the system.

DOI: [10.1103/PhysRevB.85.155412](https://doi.org/10.1103/PhysRevB.85.155412)

PACS number(s): 73.22.Pr, 72.80.Vp, 73.43.Qt, 85.30.Tv

I. INTRODUCTION

Following on the isolation of single-layer graphene, the study of bilayer graphene (BLG) became a separate direction of research in the study of two-dimensional materials. Charge carriers in bilayer graphene have a parabolic dispersion with an effective mass of about $0.054m_e$,^{1,2} but also possess a chirality. The latter manifests itself in an unconventional quantum Hall effect³ with the lowest Landau level (LLL) being eightfold degenerate. Compared to single-layer graphene, bilayer graphene has, in addition to spin and valley degrees of freedom, an orbital degree of freedom, where Landau levels with numbers $n = 0$ and 1 (each four fold degenerate) have the same energy.^{2,3} Recent advances in obtaining suspended bilayer graphene devices with charge carrier mobility exceeding $\mu > 10\,000\text{ cm}^2\text{ V}^{-1}\text{ s}^{-1}$ gave access to the investigation of many-body phenomena in clean bilayer graphene at low charge carrier concentration ($n < 10^{10}\text{ cm}^{-2}$).^{4–11}

Due to the nonvanishing density of states at the charge neutrality point (CNP), bilayer graphene is predicted to have a variety of ground states triggered by electron-electron interaction. There are two competing theories describing the ground state of BLG: a transition (i) to a gapped layer-polarized state^{12–17} (excitonic instability) or (ii) to a gapless nematic phase.^{18–20}

Excitonic instability is a layer polarization in which the charge density contribution from each valley and spin spontaneously shifts to one of the two graphene layers.^{16,17} This redistribution is caused by an arbitrarily weak interaction between charge from the conduction and valence band states.^{12,13} Since each bilayer flavor (spin or valley) can polarize toward either of the two layers, there are 16 possible states,^{16,17} which can be classified by the total polarization as being *layer* ferromagnetic (all degrees of freedom choose the same layer), *layer* ferrimagnetic (three of the four valley-spin flavors choose the same layer), or *layer* antiferromagnetic (with no overall polarization). To make it clear, the term “magnetic” should

be associated with flavor (not only spin) orientation between two layers. These states are considered as analogous to the biased bilayer²¹ in the sense that the charge transfer can be attributed to the (wave-vector-dependent) exchange potential difference between low-energy sites on the opposite layers.¹⁶ The total energy of the system is lowered by the gain in the exchange interaction via breaking of the inversion symmetry, i.e., introducing a gapped state. Antiferromagnetic polarization is electrostatically favorable due to the absence of a net charge on both layers; however, the actual ground state is theoretically undefined.^{12,16,17} Recent experiments have suggested evidence of the possible existence of two of the antiferromagnetic states—the anomalous quantum Hall (AQH) state^{5,6} and the spin-polarized layer-antiferromagnetic (LAF) state.⁷ To avoid possible confusion we note that in earlier literature¹⁶ the LAF state is also called the quantum valley Hall state. The AQH state has electrons that are polarized in the same layer for both spins and in opposite layers for opposite valleys.^{16,17} This state has spontaneously broken time-reversal symmetry and therefore possess a substantial orbital magnetization exhibiting the quantized Hall effect (at zero magnetic field), while its spin density is everywhere zero.¹⁷ Due to its magnetization the AQH state can be favored over other ground states in a perpendicular magnetic field. The LAF state has opposite spin polarization for opposite layers. In contrast to the AQH state, the LAF state does not have topologically protected edge states, which brings its minimum conductance to zero. For both states the theoretical estimations of the gap Δ give the value of 1.5–30 meV.^{13,16} However, the intervalley exchange weakly favors the LAF state.^{16,22} One of the ways to determine the character of the bilayer ground state experimentally is to investigate the response of the gap value to a magnetic field B (which couples to spin) and electrical field E (which couples to layer pseudospin).²² When Zeeman coupling is included, the AQH-state quasiparticles simply spin split, leaving the ground state unchanged but the charge gap reduced. It was calculated

that for a 4 meV spontaneous gap at zero field, a field of $B = 35$ T drives the gap to zero. On the other hand, the gap in the LAF state is weakly B field dependent.

The second possible description for the ground state of BLG is based on a nematic phase caused by the renormalization of the low-energy spectrum.^{18,19} Detailed tight-binding-model studies showed that inclusion of next-neighbor interlayer coupling changes the band structure in the bilayer, producing a Lifshitz transition in which the isoenergetic line about each valley is broken into four pockets with linear dispersion.^{2,23} At energies higher than 1 meV the four pockets merge into one pocket with the usual quadratic dispersion. Moreover, electron-electron interactions might result in further energy spectrum transformation, where the number of low-energy cones can be reduced to 2 near each of the two K points.^{18,19} In this case the minimum conductance of the bilayer graphene is supposed to be increased comparing to a bilayer with parabolic dispersion ($8e^2/h$). This scenario was also supported by experimental results on suspended bilayer graphene in which strong spectrum reconstructions and electron topological transitions were observed.¹⁰

In this paper we present electric transport properties of suspended bilayer graphene determined by studying its behavior in tilted magnetic fields. At $B = 0$ T we observe the spontaneous opening of a gap when the charge carrier density is changed from the metallic regime ($n = 3.5 \times 10^{11} \text{ cm}^{-2}$) to the CNP. At a temperature of 1 K we measure a resistance increase from 5 k Ω up to 14 M Ω . The observation indicates a gapped ground state of the studied bilayer graphene with a gap value of 6.8 meV. Measurements in a tilted magnetic field showed that the resistance at the CNP decreases with an increase of the magnetic field. Based on this we propose a possible scenario of symmetry breaking in this bilayer graphene sample: spontaneous valley splitting at zero magnetic field followed by the splitting of the spins originating from different valleys with increase of B . Both the gap value and its weak linear decrease with B support the LAF state as the ground state of the studied sample.

II. EXPERIMENTAL DETAILS

Suspended bilayer graphene devices were prepared using an acid-free technique.^{24,25} We deposited highly ordered pyrolytic graphite on an $n^{++}\text{Si}/\text{SiO}_2$ wafer (500 nm thick) which is covered with a lift-off organic resist: LOR (1.15 μm). A standard lithography procedure is performed in order to contact bilayer graphene flakes (determined by their contrast in an optical microscope) with 80 nm of Ti/Au contacts. A second electron-beam lithography step is used to expose trenches over which the graphene membrane becomes suspended. To achieve high-quality devices we use the current annealing technique by sending a dc current through the membrane (up to 1.1 mA) at a temperature of 4.2 K. While ramping up the dc current, simultaneously we keep track of the sample resistance. Once the resistance reaches values on the order of 10 k Ω we stop annealing and check the gate voltage dependence. We repeat this procedure until the appearance of a sharp resistance maximum at the CNP located close to zero V_g . More details on the current annealing procedure can be found in Tombros *et al.*²⁵ The studied device was 2 μm long and

2.3 μm wide. All measurements were performed in four-probe geometry (with contacts across the full width of graphene) at temperatures from 4.2 K down to 300 mK. The four-probe method allows the elimination of contact resistances. As discussed below the resistance measurements consist of a superposition of the longitudinal magnetoresistance (ρ_{xx}) and Hall resistance (ρ_{xy}). The carrier density in graphene is varied by applying a dc voltage (V_g) between the back gate electrode ($n^{++}\text{Si}$) and the graphene flake. Based on the serial-capacitor model, the unit capacitance of the system is 7.2 aF μm^{-2} , which relates the gate voltage with the density as $n = \alpha V_g$, where α is the leverage factor of $\alpha = 0.5 \times 10^{10} \text{ cm}^{-2} \text{ V}^{-1}$. The typical current we use is around 1 nA. See the Appendix.

III. TEMPERATURE DEPENDENCE AND QUANTUM TRANSPORT

Our pristine samples are strongly p doped with the CNP situated beyond 60 V and a metallic resistance of a few hundreds of ohms over the entire voltage range. Therefore we perform the current annealing technique in order to obtain high-quality devices. In contrast to previous samples, in which each successive step of current annealing tended to cause a sharper change in the resistance values within the scanned region of V_g , the bilayer sample discussed here already shows after the first current annealing step a highly resistive region around the CNP (not shown). The next annealing step (1.1 mA) moves the charge neutrality point down to $V_g = 1.2$ V. However, surprisingly, the resistance around the CNP becomes 14 M Ω and is reduced down to 5 k Ω in the metallic regime at $V_g = -60$ V [Fig. 1(a), inset]. This fact points toward opening of a gap. The temperature dependence of the membrane from 4.2 K to 300 mK is shown in Fig. 1(a). There is an essential change of about 6 M Ω in the maximum resistance (R_{max}) from 4.2 down to 1.3 K; however, further lowering of the temperature does not change R_{max} much. From an Arrhenius plot of the resistance at the CNP [Fig. 1(c)] we can extract a thermal excitation gap of 0.33 meV.²⁶ The saturation of resistance at lower T can be explained by variable-range hopping with different temperature dependence. We would like to point out that our excitation current value of 1 nA gave a voltage drop around 10 mV at the CNP, which is much higher than the energy kT at measured temperatures (0.3 meV). Therefore one has to be careful in comparing transport and thermal excitation gaps.

There might be several scenarios for the observed gap formation in the gate voltage dependence: (i) A lateral confinement in the membrane, where the energy levels are

$$E_n = \frac{\hbar^2 k^2}{2m} = \frac{\hbar^2 \pi^2}{2m W^2} l^2. \quad (1)$$

$W = 2.3 \mu\text{m}$ is the width of the flake and l is an integer. However, the first two levels have energies of $E_1 = 1.3 \mu\text{eV}$ and $E_2 = 5.3 \mu\text{eV}$, which are much lower than $k_B T$ at measured temperatures. (ii) True gap formation with zero density of states within the gap and available states at the conduction and valence bands. (iii) A transport gap, accompanied by observation of reproducible conductance oscillations in the region of suppressed conductance. In such a

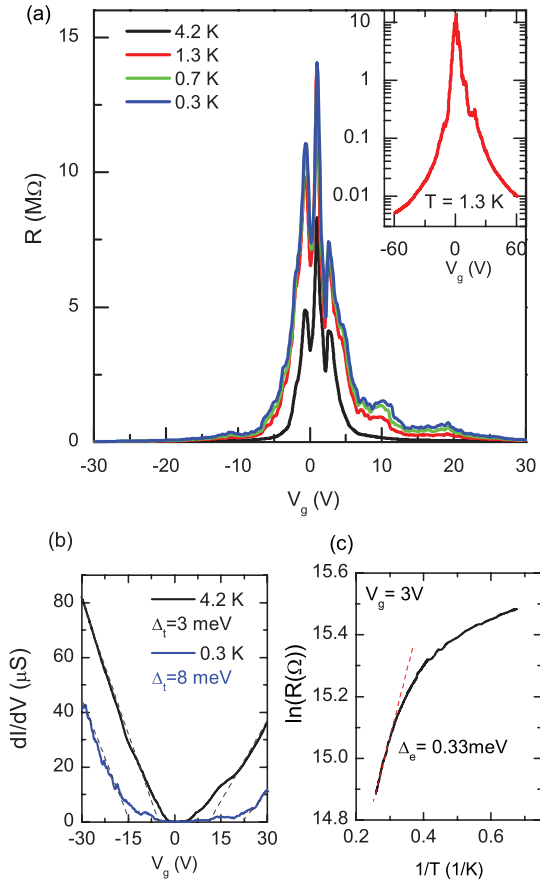


FIG. 1. (Color online) Four-probe resistance of the suspended bilayer graphene. (a) Gate dependence of the sample at the temperatures of 4.2 (black), 1.3 (red), 0.7 (green), and 0.3 K (blue). Inset: Resistance at 4.2 K on a logarithmic scale showing the dramatic change from the CNP to the metallic regime. (b) Transport gap extraction at 4.2 and 0.3 K. The energy gap in the bias direction is highlighted by the conductance crossover (fitted with dashed lines) at zero. The values of the transport gap are 3 meV (4.2 K) and 8 meV (0.3 K). (c) An Arrhenius plot of the resistance. The value of the extracted thermal gap is 0.33 meV.

regime transport is limited by the quantum confinement effect along the width (mainly originating from the impurities).²⁷ (iv) A more complicated case, when the gap value depends on the charge carrier density, i.e., the energy of the levels changes while they are being filled with carriers. This situation might happen when the gap is induced by charge redistribution between layers, which would be influenced by the applied back gate voltage. At the moment, we cannot determine the exact gap type; therefore, further analysis is performed assuming a transport gap scenario, but keeping in mind that this gap value can depend on the density.

In analogy to graphene nanoribbon studies,^{27,28} we extract the transport gap from the gate dependence of the sample conductance as shown in Fig. 1(b). From a linear approximation of conductance, one gets a region of ΔV_g where the sample shows insulating behavior. This region ΔV_g relates to the wave vector as $\Delta k = \sqrt{\pi \Delta n} = \sqrt{\pi \alpha \Delta V_g}$. Taking into account the quadratic dispersion of bilayer graphene, the corresponding

energy scale can be calculated as

$$\Delta E_F = \frac{\hbar^2 k^2}{2m} = \frac{\hbar^2}{2m} \pi \alpha \Delta V_g. \quad (2)$$

From conductance graphs at different T we find $\Delta E_F = 3$ meV at 4.2 K and $\Delta E_F = 8$ meV at 0.3 K. The values of the transport gap are comparable to the energy gap (extracted in the bias direction) values of single-layer graphene nanoribbons of 50–85 nm wide,^{27,28} where in contrast to our case the gap is created by lateral confinement. The resistance value of 5 k Ω in the metallic regime, similar to that of regular graphene devices, serves as an additional justification for excluding lateral confinement as a cause of the observed transport gap. We can calculate the mobility of the charge carriers using the standard formula $\mu = 1/(eR_{sq}n)$, where R_{sq} is the square resistance of the sample and e is the elementary charge. The mobility value $\mu \propto 20\,000$ cm² V⁻¹ s⁻¹ at $n = 3.5 \times 10^{11}$ cm⁻² corresponds to the value of high quality bilayer graphene devices. Due to the symmetry of resistance change around the CNP [Fig. 1(b)] and the fact that the CNP itself is situated around zero gate voltage ($V_g = 1.2$ V), which corresponds to the density of $n = 0.77 \times 10^{10}$ cm⁻² at 0 V, we can also exclude the low-quality “ p -doped” regions close to the contacts (which can form after current annealing) as the cause of the reported gap. In the meantime, we cannot exclude a charge inhomogeneity in the sample bulk which might lead to the observed order of magnitude difference between electrical and transport gaps, in analogy to the nanoribbon case.

Given the fact that the resistance reaches M Ω values at the CNP, it is already hard to establish quantum Hall plateaus in our suspended bilayer device. However, we have achieved the observation of quantum Hall transport shown in Figs. 2(a) and 2(b). The first quantum Hall plateau appears at 5 T on the hole side (red curve), which we attribute to the filling factor $\nu = 2$. This plateau is followed by the appearance of $\nu = 1$ at 7 T [Fig. 2(b)]. The conductance values of the observed plateaus deviate from the expected ones of $2e^2/h$ and $1e^2/h$, since they are affected by charge inhomogeneity. Therefore, we determine the exact values of the corresponding plateaus by the scaling of their positions in the graph of density (V_{gv}) vs magnetic field B [Fig. 2(d)]. As expected from $\nu = n/(eB/h)$ the scaling is linear with the leverage factor of $\alpha = 0.64 \times 10^{10}$ cm⁻² V⁻¹ for $\nu = 2$ and 1. In order to use the same α for both filling factor sets [see Fig. 2(d)] the slopes of V_{gv} versus B and the ν values, respectively, have to be a factor of 2 different. Therefore, we have to point out that the linear scaling will hold as well for a leverage factor of 1.1×10^{10} cm⁻² V⁻¹ if we assume $\nu = 4$ and 2 as the observed sequence of plateaus. From previous studies²⁹ we know that the capacitance probed by the quantum Hall effect (QHE) in graphene devices (especially in suspended samples) can be higher than the geometrical value, due to the deviation from the plane capacitor model. However, we attribute the observed plateaus to the filling factors 2 and 1. As we noticed before,^{8,24} most of the time the current annealing procedure leads to the formation of high-quality annealed regions connected in series with low-mobility p -doped regions close to the contacts. Therefore higher values of the conductance plateaus can be explained by a p -doped slope, which increases with magnetic

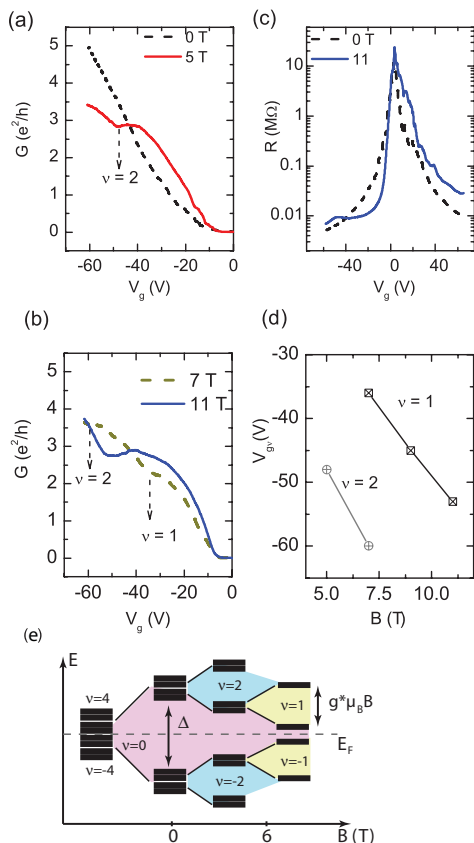


FIG. 2. (Color online) Quantum transport at 1.3 K. (a) Quantum Hall conductance of the suspended bilayer at $B = 0$ and 5 T. (b) Quantum Hall conductance of the suspended bilayer at $B = 7$ and 11 T. The exact filling factors ν corresponding to the observed plateaus are shown. (c) Resistance of the sample in the quantum Hall regime. (d) Scaling of the filling factor positions in graph of gate voltage (V_{gv}) vs magnetic field. (e) LL hierarchy of the symmetry breaking of the lowest LL in bilayer graphene. Suggested scenario of spontaneous valley splitting followed by spin splitting at high B .

field B . This might also be the reason for the absence of resistance quantization on the electron side [Fig. 2(c)]. Assuming $\mu B \gg 1$ for the formation of QHE plateaus,³⁰ our observation implies a lower bound for the mobility of $2000 \text{ cm}^2 \text{ V}^{-1} \text{ s}^{-1}$.

To summarize our QH transport results: At this point we have shown that a zero-field gap opens at the CNP in the studied graphene bilayer. This observation points to a possible symmetry breaking of the ground state in bilayer graphene. The application of B does not restore the broken symmetry and brings the system into the QH regime. In Fig. 2(e) we show the hierarchy of the splitting of the eightfold-degenerate lowest Landau level in applied B .³¹ The development of the level structure with B will be specified and discussed in Sec. IV. Meanwhile, if we assume that at $B = 0$ T one of the degeneracies is already lifted, then, with increasing field, one can expect quantization at the filling factors $\nu = 0$ and 4 followed by $\nu = 2$ and 1. However, if the initial symmetry breaking is strong enough and the scanned window in energy is limited (V_g), then one can expect quantization at $\nu = 2$ followed by $\nu = 1$. This described hierarchy of level splitting

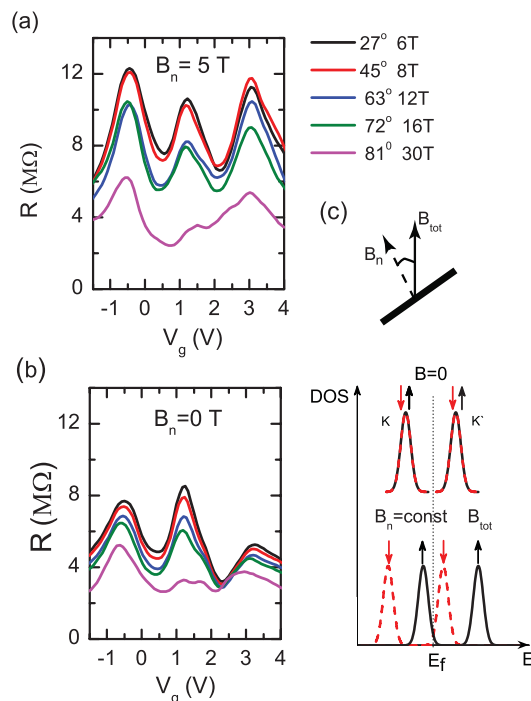


FIG. 3. (Color online) (a) Behavior of the resistance at the charge neutrality point at fixed B_n with increasing B_{tot} . From top to bottom, angle and total field are 27° (6 T), 45° (8 T), 63° (12 T), 27° (6 T), 72° (16 T), and 81° (30 T). (b) Behavior of the resistance at the charge neutrality point when B has only the in-plane field component ($\theta = 90^\circ$). (c) Suggested scheme of spontaneously split valley followed by spin splitting induced by B .

and sequence of plateaus will be observed independent of whether valley or spin splitting occurs first.

IV. RESISTANCE AT THE CNP IN TILTED MAGNETIC FIELD

In order to clarify the nature of the gapped ground state of bilayer graphene and its evolution in a magnetic field we perform a tilted-magnetic-field experiment. In tilted experiments the total magnetic field (B_{tot}) can be separated from its normal (to the plane of the sample) component: $B_n = B_{tot} \cos \theta$, where θ is the angle between these two vectors [Fig. 3(c)]. This procedure allows us to distinguish between the orbital effect (QHE) and pure Zeeman energy, which has to scale with the B_{tot} value.^{22,31,32}

All measurements presented below were performed at a temperature of 1.3 K. The application of the magnetic field perpendicular to the sample plane leads to an increase in the resistance at the CNP, as expected for QH transport in the case of broken-symmetry states. To distinguish between the normal component and total B we perform a series of experiments keeping B_n fixed and gradually increasing B_{tot} . As an example, in Fig. 3(a) we show the change in R_{max} at $B_n = 5$ T with B_{tot} increasing from 6 to 30 T for different angles θ . The actual maximum of the resistance consists of three peaks: highly resistive in the middle ($V_g = 1.2$ V) and two side peaks at the gate voltages at -0.5 and 3 V. The total magnetic field causes

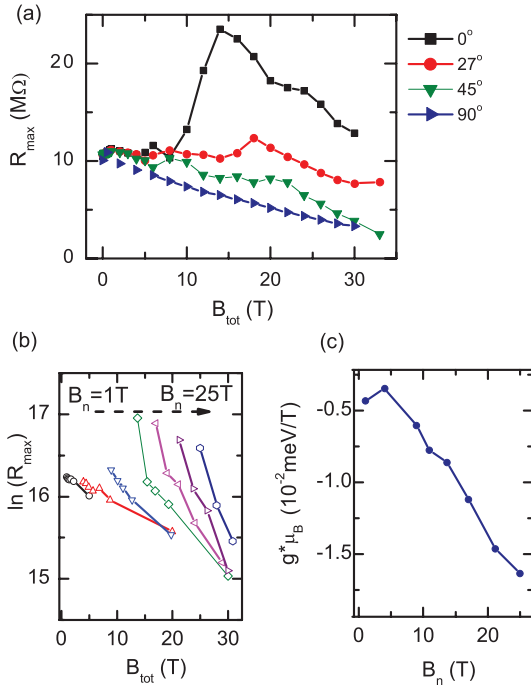


FIG. 4. (Color online) (a) Change in the R_{\max} of the middle peak with total magnetic field B_{tot} . (b) $\ln(R_{\max})$ as a function of B_{tot} at different B_n . The values of B_n from left to right are 1, 4, 9, 13.7, 17, 21.2, and 25 T. (c) The slope of the linear fit from (b) as a function of the normal component B_n .

a decrease in the resistance and the middle peak starts splitting into two peaks (or developing a minimum in resistance at the CNP) when $B_{\text{tot}} > 6$ T for studied values of B_n . We observe exactly the same behavior in the experiment when $B_n = 0$ and the applied field is parallel to the graphene membrane: the maximum of the resistance goes down and develops a local minimum at the CNP [Fig. 3(b)]. We attribute this change to an increase of the total magnetic field. The fact that the resistance changes with B_{tot} indicates that the observed effect is not a simple quantum localization due to inhomogeneity in the sample.

All three maxima around the CNP decrease in their resistance in a parallel applied B . However, only the middle maximum at $V_g = 1.2$ V shows clear scaling with the total magnetic field (B_{tot}) at different tilt angles θ [Fig. 4(a)]. As one can see in the case of $B_{\text{tot}} = B_n$ [$\theta = 0$, black curve in Fig. 4(a)] the resistance keeps on increasing up to around 14 T; further increase in the magnetic field brings R_{\max} to lower values [Fig. 4(a)]. Once the nonzero angle is introduced the common trend for R_{\max} is a decrease.

We suggest that the behavior of the middle peak is caused by a many-body effect and can be explained by the Zeeman splitting closing the spontaneous gap. The hierarchy of energy levels is depicted in Fig. 2(e). Once B is large enough the LLL is split into four levels, each twofold degenerate. If we assume that the latter degeneracy is that of spin, then after the appearance of the plateau associated with filling factor $\nu = 1$ we expect the value of the ground-state gap Δ to be lowered by spin splitting coupled to B_{tot} . Here we would like to emphasize that we do observe the appearance of $\nu = 1$ and a minimum of resistance at the CNP in a similar magnetic field $B_{\text{tot}} > 7$ T. In

a simplified way we describe the resistance value at the CNP point as

$$\ln R_{\max} \propto \Delta/(kT) - g^* \mu_B B_{\text{tot}}/(kT), \quad (3)$$

where g^* is an effective g factor including exchange electron interaction and a Landau level broadening.^{8,32,33} The change in $\ln(R)$ versus B_{tot} at fixed B_n values is shown in Fig. 4(b). This dependence can be best described as linear. The slope and y intercept of the linear fit of Fig. 4(b) give the values of Δ and $g^* \mu_B$. Surprisingly, both these contributions scale with the B_n component. In Fig. 4(c) we show $g^* \mu_B$ versus B_n . Despite the fact that the scaling appears linear, a plot of the slope as a function of $\sqrt{B_n}$ does seem to fit also (not shown). Δ increases with B_n from 1.4 meV at $B_n = 1$ T up to 1.7 meV at $B_n = 25$ T (not shown). This Δ is of the same order as the measured transport gap (which can overestimate the real energy gap) and also corresponds to the theoretically predicted gap of 1.5–30 meV for the excitonic instability.^{13,16,22}

In summary, tilted-magnetic-field experiments show that the resistance at the CNP of the studied gapped bilayer graphene decreases linearly with increase of the total magnetic field component. This points to a many-body effect and weak reduction of the gap in an applied magnetic field. The developed minimum in the resistivity in Fig. 3 can be explained by the overlapping of spin-up and spin-down levels from the adjacent Landau levels due to Zeeman splitting in the applied B .³³ However, from our experiments the estimated $g^* < 0.2$, which is very low for spin splitting. In addition, although the resistance decreases in a parallel field, the R_{\max} value does not change by an order of magnitude. This behavior in B is consistent with the layer-antiferromagnetic state being the ground state of the studied bilayer sample.²² Since in this state the top and bottom layers host spins with opposite orientations, their interaction with the applied B cannot be described as a simple Zeeman splitting. Our results also open an additional question: What is the role of exchange energy and level broadening Γ in the LAF state? Naively, the scaling of $g^* \mu_B$ with B_n can be understood from their dependence on the level broadening Γ . The Γ value scales with $\sqrt{B_n}$, meaning that for bigger B_n a smaller B_{tot} is needed to observe overlapping of the levels. In reality the situation can be much more complicated, including possible exchange mechanisms that we do not understand yet. This is also supported by the fact that the ground-state gap Δ depends on B_n as well.

Based on these results we suggest a possible scenario of symmetry breaking in high-quality bilayer graphene [Figs. 2(e) and 3(c)]. The first splitting is caused by valleys and results in the observed transport gap. Application of a magnetic field induces spin splitting of both K and K' levels. When B is high enough then the energy of the spin-up level from K will start approaching the spin-down level from K' . The overlapping of the levels will cause a decrease in the resistance at the charge neutrality point. Since we do observe a transport gap in our sample, we exclude a nematic phase transition. In addition to this, the response of the sample in tilted B fits the LAF state. The cause of the valley splitting can be a combination of two effects: electron-electron interaction (which determines the B field behavior of the middle resistance maximum) and a contamination of the sample surface with charged impurities

which breaks inversion symmetry (via the introduction of an electrical field).²¹

V. CONCLUSIONS

We report a transport gap of 3 meV in suspended bilayer graphene at 4.2 K, which increases with decreasing temperature. The sequence of appearance of the QHE plateaus at the filling factor $\nu = 2$ followed by $\nu = 1$ supports the suggestion that the observed gap is caused by symmetry breaking. Measurements in a tilted magnetic field indicate that the resistance at the CNP shows a weak linear decrease with increase in the total magnetic field. Based on this we propose a possible scenario for the symmetry breaking in the investigated bilayer graphene: spontaneous valley splitting at zero magnetic field followed by the splitting of spins originating from different valleys with increase of B . The gap value and weak response of the sample to applied magnetic field correspond to the predicted spin-polarized layer-antiferromagnetic state as the ground state of the investigated sample. The observed non-trivial dependence of the gap value on the normal component of B suggests possible exchange mechanisms in the system.

ACKNOWLEDGMENTS

We would like to thank B. Wolfs, M. de Roos, and J. G. Holstein for technical assistance. We also thank M. H. D. Guimarães for useful discussions, and I. J. Vera-Marun for creating a software program for current annealing. This work is supported by NWO (via a TopTalent grant), FOM, NanoNed, and the Zernike Institute for Advanced Materials.

APPENDIX

In order to minimize self-heating in graphene at the high-resistance CNP we used the following scheme (Fig. 5).

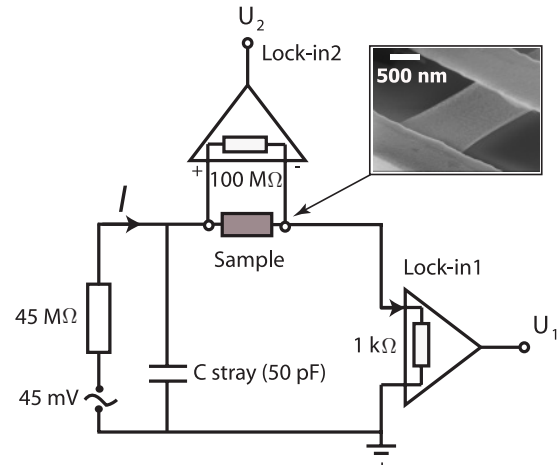


FIG. 5. (Color online) Electrical scheme of the setup we use to perform our measurements. Inset: Scanning electron micrograph of a typical suspended bilayer membrane between two contacts.

An ac source maintained a fixed voltage amplitude of 45 mV (1.87 Hz frequency) across the sample in series with a 45 MΩ resistor. The current through the sample is monitored by the lock-in 1, whose output U_1 is proportional to the current flowing in the circuit ($U_1 = I \times 1 \text{ k}\Omega$). Simultaneously, the four-probe voltage across the sample (U_2) is phase detected by another lock-in 2 connected through the preamplifier and having an input resistance up to 100 MΩ. Then the resistance of the sample is determined by $R = 1 \text{ k}\Omega \times U_2/U_1$. The power dissipating in the sample is $P = U_2^2/R$. Therefore, assuming that the maximum U_2 is already reached ($\propto 10 \text{ mV}$), with increase of R the dissipation in the sample will decrease.

*a.veligura@rug.nl

¹E. McCann, *Phys. Rev. B* **74**, 161403 (2006).

²E. McCann and V. I. Fal'ko, *Phys. Rev. Lett.* **96**, 086805 (2006).

³K. S. Novoselov, E. McCann, S. V. Morozov, V. I. Fal'ko, M. I. Katsnelson, U. Zeitler, D. Jiang, F. Schedin, and A. K. Geim, *Nat. Phys.* **2**, 177 (2006).

⁴B. E. Feldman, J. Martin, and A. Yacoby, *Nat. Phys.* **5**, 889 (2009).

⁵R. T. Weitz, M. T. Allen, B. E. Feldman, J. Martin, and A. Yacoby, *Science* **330**, 812 (2010).

⁶J. Martin, B. E. Feldman, R. T. Weitz, M. T. Allen, and A. Yacoby, *Phys. Rev. Lett.* **105**, 256806 (2010).

⁷J. J. Velasco, L. Jing, W. Bao, Y. Lee, P. Kratz, V. Aji, M. Bockrath, C. Lau, C. Varma, R. Stillwell, D. Smirnov, F. Zhang, J. Jung, and A. MacDonald, *Nat. Nanotechnol.* **7**, 156 (2012).

⁸H. J. van Elferen, A. Veligura, E. V. Kurganova, U. Zeitler, J. C. Maan, N. Tombros, I. J. Vera-Marun, and B. J. van Wees, *Phys. Rev. B* **85**, 115408 (2012).

⁹F. Freitag, J. Trbovic, M. Weiss, and C. Schönberger, *Phys. Rev. Lett.* **108**, 076602 (2012).

¹⁰A. S. Mayorov, D. C. Elias, M. Mucha-Kruczynski, R. V. Gorbachev, T. Tudorovskiy, A. Zhukov, S. V. Morozov, M. I. Katsnelson, V. I. Fal'ko, A. K. Geim, and K. S. Novoselov, *Science* **33**, 860 (2011).

¹¹W. Bao, J. Velasco, F. Zhang, L. Jing, B. Standley, D. Smirnov, M. Bockrath, A. MacDonald, and C. N. Lau, e-print [arXiv:1202.3212](https://arxiv.org/abs/1202.3212).

¹²R. Nandkishore and L. Levitov, *Phys. Rev. Lett.* **104**, 156803 (2010).

¹³R. Nandkishore and L. Levitov, *Phys. Rev. B* **82**, 115431 (2010).

¹⁴H. Min, G. Borghi, M. Polini, and A. H. MacDonald, *Phys. Rev. B* **77**, 041407 (2008).

¹⁵F. Zhang, H. Min, M. Polini, and A. H. MacDonald, *Phys. Rev. B* **81**, 041402 (2010).

¹⁶J. Jung, F. Zhang, and A. H. MacDonald, *Phys. Rev. B* **83**, 115408 (2011).

¹⁷F. Zhang, J. Jung, G. A. Fiete, Q. Niu, and A. H. MacDonald, *Phys. Rev. Lett.* **106**, 156801 (2011).

¹⁸O. Vafek and K. Yang, *Phys. Rev. B* **81**, 041401 (2010).

¹⁹Y. Lemonik, I. L. Aleiner, C. Toke, and V. I. Fal'ko, *Phys. Rev. B* **82**, 201408 (2010).

- ²⁰C. Tóke and V. I. Fal'ko, e-print [arXiv:0903.2435](https://arxiv.org/abs/0903.2435).
- ²¹E. V. Castro, K. S. Novoselov, S. V. Morozov, N. M. R. Peres, J. M. B. Lopes dos Santos, J. Nilsson, F. Guinea, A. K. Geim, and A. H. Castro Neto, *Phys. Rev. Lett.* **99**, 216802 (2007).
- ²²F. Zhang and A. H. MacDonald, e-print [arXiv:1107.4727](https://arxiv.org/abs/1107.4727) [*Phys. Rev. Lett.* (to be published)].
- ²³E. McCann, D. S. Abergel, and V. I. Fal'ko, *Solid State Commun.* **143**, 110 (2007).
- ²⁴N. Tombros, A. Veligura, J. Junesch, J. J. van den Berg, P. J. Zomer, M. Wojtaszek, I. J. Vera-Marun, H. T. Jonkman, and B. J. van Wees, *J. Appl. Phys.* **109**, 093702 (2011).
- ²⁵N. Tombros, A. Veligura, J. Junesch, M. H. D. Guimaraes, I. J. Vera-Marun, H. T. Jonkman, and B. J. van Wees, *Nat. Phys.* **7**, 697 (2011).
- ²⁶F. Xia, D. B. Farmer, Y.-m. Lin, and P. Avouris, *Nano Lett.* **10**, 715 (2010).
- ²⁷F. Molitor, C. Stampfer, J. Güttinger, A. Jacobsen, T. Ihn, and K. Ensslin, *Semicond. Sci. Technol.* **25**, 034002 (2010).
- ²⁸C. Stampfer, J. Güttinger, S. Hellmüller, F. Molitor, K. Ensslin, and T. Ihn, *Phys. Rev. Lett.* **102**, 056403 (2009).
- ²⁹I. J. Vera-Marun, P. Zomer, A. Veligura, M. H. D. Guimaraes, L. Visser, N. Tombros, H. J. van Elferen, U. Zeitler, and B. J. van Wees, e-print [arXiv:1112.5462](https://arxiv.org/abs/1112.5462).
- ³⁰K. I. Bolotin, K. J. Sikes, Z. Jiang, M. Klima, G. Fudenberg, J. Hone, P. Kim, and H. L. Stormer, *Solid State Commun.* **146**, 351 (2008).
- ³¹Y. Zhao, P. Cadden-Zimansky, Z. Jiang, and P. Kim, *Phys. Rev. Lett.* **104**, 066801 (2010).
- ³²E. V. Kurganova, H. J. van Elferen, A. McCollam, L. A. Ponomarenko, K. S. Novoselov, A. Veligura, B. J. van Wees, J. C. Maan, and U. Zeitler, *Phys. Rev. B* **84**, 121407 (2011).
- ³³R. J. Nicholas, R. J. Haug, K. v. Klitzing, and G. Weimann, *Phys. Rev. B* **37**, 1294 (1988).